PCCP

ROYAL SOCIETY OF CHEMISTRY

PAPER

View Article Online
View Journal | View Issue

Cite this: *Phys. Chem. Chem. Phys.*, 2023, **25**, 32549

Two-dimensional III-nitride alloys: electronic and chemical properties of monolayer $Ga_{(1-x)}Al_xN$†

Yiqing Chen, [a] Ying Zhao, [a] Pengfei Ou *[ab] and Jun Song *[a]

Received 12th July 2023,
Accepted 15th November 2023

DOI: 10.1039/d3cp03291d

rsc.li/pccp

Potential applications of III-nitrides have led to their monolayer allotropes, *i.e.*, two-dimensional (2D) III-nitrides, having attracted much attention. Recently, alloying has been demonstrated as an effective method to control the properties of 2D materials. In this study, the stability, and the electronic and chemical properties of monolayer $Ga_{(1-x)}Al_xN$ alloys were investigated employing density functional theory (DFT) calculations and the cluster expansion (CE) method. The results show that 2D $Ga_{(1-x)}Al_xN$ alloys are thermodynamically stable and complete miscibility in the alloys can be achieved at ambient temperature (>85 K). By analyzing CE results, the atomic arrangement of 2D $Ga_{(1-x)}Al_xN$ was revealed, showing that Ga/Al atoms tend to mix with the Al/Ga atoms in their next nearest site. The band gaps of $Ga_{(1-x)}Al_xN$ random alloys can be tuned by varying the chemical composition, and the corresponding bowing parameter was calculated as −0.17 eV. Biaxial tensile strain was also found to change the band gap values of $Ga_{(1-x)}Al_xN$ random alloys ascribed to its modifications to the CBM positions. The chemical properties of $Ga_{(1-x)}Al_xN$ can also be significantly altered by strain, making them good candidates as photocatalysts for water splitting. The present study can play a crucial role in designing and optimizing 2D III-nitrides for next-generation electronics and photocatalysis.

Introduction

III-Nitrides, including AlN, GaN and InN and their alloys, are promising semiconductors that possess tunable band gaps covering the spectral range from ultraviolet to infrared.[1,2] The excellent properties of III-nitrides have made them ideal candidate materials for modern electronic and optoelectronic devices.[2,3] Meanwhile, due to their unique surface properties, III-nitrides exhibit great potential in photocatalysis and have recently gained importance in the hydrogen evolution reaction, oxygen evolution reaction and carbon dioxide reduction.[4–7]

The wide-ranging applications of III-nitrides have also brought their monolayer allotropes, *i.e.*, two-dimensional (2D) III-nitrides, into the focus of research interest. 2D III-nitrides were first predicted using first-principles calculations,[8] and then synthesized *via* graphene encapsulation.[9] 2D III-nitrides were found to have different forms, among which graphene-like planar GaN and AlN (2D hexagonal GaN and AlN) were extensively studied.[10,11] Previous works demonstrated the stability of 2D hexagonal GaN and AlN from *ab initio* phonon calculations.[12,13] Additionally, 2D hexagonal GaN and AlN were found to retain their stability under thermal excitations as confirmed by *ab initio* finite temperature molecular dynamics (MD) calculations performed under 1000 K.[14] Similar to bulk semiconductors, 2D III-nitrides have demonstrated desirable properties for a broad range of applications. For example, the band gap of 2D hexagonal GaN can be tailored by decorating with H or F adatoms, showing potential for optoelectronic devices;[15] the 2D GaN/$Mg(OH)_2$ heterostructure was predicted to have suitable band structures and adsorption abilities that promote water splitting.[16]

However, the low stability of 2D III-nitrides is a bottleneck for their applications.[8] Since their bulk counterparts do not have layered structures like graphite, the fabrication of layered III-nitrides inevitably introduces unsaturated dangling bonds on the surface, which makes the synthesis difficult and thus hampers their large-scale applications. Modification strategies are required to overcome the limitations and tune the physical and chemical properties of 2D III-nitrides. Recent research has shown that alloying can be an effective strategy in 2D materials to enhance the thermodynamic stability and achieve tunable electronic and optical properties.[17,18] 2D alloys like $Mo_{(1-x)}W_xS_2$ and $Mo_{(1-x)}W_xSe_2$ were found to exhibit negative formation energies, which indicate that alloying can successfully stabilize 2D structures.[17] Among the III-nitrides, Kanli *et al.* investigated the dynamical stability and band gap bowing of 2D $Ga_{(1-x)}Al_xN$ ordered alloys;[19] Wines *et al.* demonstrated the electronic and thermoelectric properties of 2D $B_{(1-x)}Al_xN$,

[a] *Department of Mining and Materials Engineering, McGill University, 3610 University St, Montreal, QC H3A 0C5, Canada. E-mail: pengfei.ou@northwestern.edu, jun.song2@mcgill.ca*
[b] *Department of Chemistry, Northwestern University, 2145 Sheridan Rd, Evanston, IL 60208, USA*

† Electronic supplementary information (ESI) available. See DOI: https://doi.org/10.1039/d3cp03291d

$Al_{(1-x)}Ga_xN$, and $Ga_{(1-x)}In_xN$ alloys.[10] Despite those great prior efforts, several aspects of 2D III-nitride alloys remain not well understood, *i.e.*, the atomic ordering of alloy structures and the band gap bowing effect for random alloys. In addition, the strain effect to the electronic properties and the chemical properties of 2D $Ga_{(1-x)}Al_xN$ have not been explored yet.

In light of the above limitations, the present study investigated the stability, electronic and chemical properties of monolayer $Ga_{(1-x)}Al_xN$ alloys employing density functional theory calculations (DFT) and the cluster expansion (CE) method. The stability of 2D $Ga_{(1-x)}Al_xN$ alloys was examined and the atomic arrangement of alloys was revealed. We found that 2D $Ga_{(1-x)}Al_xN$ alloys are thermodynamically stable, and the complete miscibility in alloys can be achieved at ambient temperature. Using random alloy structures, the electronic properties of 2D $Ga_{(1-x)}Al_xN$ alloys were then investigated, with the band gap bowing parameter calculated to be −0.17 eV. Biaxial tensile strain was then applied to study their effect to the band gap values and chemical properties of 2D $Ga_{(1-x)}Al_xN$ alloys, with continuously tunable properties observed by varying chemical composition. Our work may guide the future design of 2D $Ga_{(1-x)}Al_xN$ alloys in electronics and photocatalysis.

Computational methods

Cluster expansion

In the CE formalism,[20,21] each metal site in an alloy configuration is assigned an occupation variable σ_i, with σ_i being equal to +1 or −1, representing which species is present at this site (*e.g.*, +1 for Ga, and −1 for Al). In this way, any alloy configuration can be well described by a vector $\vec{\sigma} = (\sigma_1, \sigma_1, \sigma_1, \ldots)$ containing all the σ_i information of the lattice. As a result, the formation enthalpy of a particular alloy configuration is expressed as[22,23]

$$\Delta H\left(\vec{\sigma}\right) = \sum_{\alpha} m_\alpha J_\alpha \xi_\alpha\left(\vec{\sigma}\right)$$

where α denotes a cluster, including singles, pairs and triplets. m_α is the number of symmetry-equivalent clusters of α, and J_α is the effective cluster interaction (ECI) parameter, representing the energy contribution from cluster α. The summation is taken over all symmetry-non-equivalent clusters. ξ_α is the cluster correlation function defined as

$$\xi_\alpha\left(\vec{\sigma}\right) = \left\langle \prod_{i\in\alpha'} \sigma_i \right\rangle$$

with the angle bracket representing the average of the spin product of all symmetry-equivalent clusters α' of α. The ECIs are determined by fitting a certain number of samples obtained from density functional theory (DFT) calculations, and the fitted ECIs can then be used to predict the formation enthalpies of any alloy configuration quickly by just calculating the ξ_α.

In this work, the CE method was employed using the Alloy-Theoretic Automated Toolkit (ATAT) code to fit the formation enthalpies of $Ga_{(1-x)}Al_xN$ alloys.[22] The formation enthalpies of 70 ordered structures up to 22 atoms per cell were calculated from density functional theory (DFT) calculations, and then were used to fit the ECI values. The performance of the CE fitting was evaluated by cross-validation score with values of around 0.1 meV. The fitted ECIs were then used to predict the formation enthalpies of more than 1000 $Ga_{(1-x)}Al_xN$ alloy configurations.

Special quasi-random structure (SQS) method

SQS method was applied to investigate the stability and electronic properties of totally disordered $Ga_{(1-x)}Al_xN$ alloys.[24] For a random alloy, the correlation function is defined as $(2x-1)^k$, with x the concentration of alloy and k the number of metal sites in the cluster (*e.g.*, k = 2 for pairs.).[24] The SQS method generates special structures that have correlation functions close to random alloys, then these SQS structures can be used to simulate the physical properties of random alloys. In this study, SQS structures were constructed in 6 × 6 supercells for x = 1/6, 1/3, 1/2, 2/3, and 5/6.

Free energy of random alloys

The free energy of random alloys $F(x, T)$ is temperature-dependent and can be analytically estimated using the following equation:

$$F(x,T) = \Delta H(x) - TS(x)$$

Here, $\Delta H(x)$ is the formation enthalpy obtained from DFT calculations and T is the temperature. $S(x)$ is the entropy and can be estimated using a mean-field approach, which is defined as[23,25]

$$S(x) = -k_B[x\ln x + (1-x)\ln(1-x)]$$

where k_B is the Boltzmann constant. Positive and negative free energies indicate immiscible and miscible alloys, and the miscibility of alloys is tunable by increasing the temperature. The above equations can be used to estimate the critical temperature for complete miscibility (T_{CM}) of random alloys.

Gibbs free energy of adsorption

Based on the computational hydrogen electrode (CHE) model,[26] the Gibbs free energy of adsorption ΔG was calculated *via*

$$\Delta G = E_{ad} + \Delta ZPE - T\Delta S \quad \text{(S1)}$$

where E_{ad} is the adsorption energy calculated as

$$E_{ad} = E_{surface+adsorbate} - E_{surface} - E_{adsorbate} \quad \text{(S2)}$$

ΔZPE and ΔS are the changes in zero-point energy and entropy during adsorption, and T is the room temperature set as 298 K.

DFT calculations

Spin-polarized DFT calculations[27] were performed employing the Vienna *Ab Initio* Simulation Package (VASP).[28,29] The interactions of electrons with ion cores were represented *via* the projector-augmented wave (PAW) method,[30] and the exchange–correlation was described by the Perdew–Burke–Ernzerhof (PBE) functional.[31,32] To obtain more accurate band gap values, the hybrid Heyd–Scuseria–Ernzerhof (HSE06) functional was

implemented for the calculation of electronic properties.[33] A kinetic cutoff energy of 550 eV was set for the plane-wave basis functions. To avoid periodic image interactions, a vacuum layer of at least 15 Å was set along the layer direction for all the structures. All structures were relaxed until the residual forces were smaller than 0.02 eV $Å^{-1}$ and the electronic energy converged to 10^{-5} eV. For alloys generated for CE fitting, the *k*-point density was 1000 K points per reciprocal atom; for SQS structures with larger supercells, a *Γ*-centered *k*-point mesh of $2 \times 2 \times 1$ was used. For the calculations of the adsorption, the effect of van der Waals (vdW) interactions was considered using the DFT-D3 method.[34,35]

Results and discussion

Configurations and stabilities of $Ga_{(1-x)}Al_xN$ alloys

We start from 2D GaN and AlN with graphene-like planar honeycomb structures. The optimized structures of 2D hexagonal GaN and AlN are presented in Fig. 1, with lattice constants calculated to 3.21 Å and 3.13 Å respectively, comparable to those reported in the previous theoretical studies.[19,36] 68 unique 2D $Ga_{(1-x)}Al_xN$ alloy configurations in the whole concentration range were then generated based on the pristine structures and optimized using PBE functionals. After structural optimization, $Ga_{(1-x)}Al_xN$ alloys retain their original hexagonal planar cell shape (see examples of $Ga_{(1-x)}Al_xN$ in Fig. S1 in the ESI†). Due to such small lattice distortion in the structures, it is expected that the standard CE method can properly match the structures and accurately fit the formation enthalpies of $Ga_{(1-x)}Al_xN$ alloys.[37]

Fig. 2(a) shows the CE simulated results for 2D $Ga_{(1-x)}Al_xN$ alloys. The formation enthalpies ΔH for all alloy configurations are positive, which indicates that no $Ga_{(1-x)}Al_xN$ alloy structures can be stable at 0 K. We also constructed a series of SQS structures representing random alloys at concentrations of x = 1/6, 1/3, 1/2, 2/3 and 5/6, with corresponding optimized configurations shown in Fig. 2(c) and calculated ΔH plotted in Fig. 2(a). As demonstrated, random alloys also have positive ΔH that lies within the range of CE predicted values. This implies that $Ga_{(1-x)}Al_xN$ random alloys are also unstable and have the tendency of segregation at 0 K. To understand the relationship between atomic arrangement and the ΔH, the fitted ECI parameters were analyzed and are presented in Fig. 2(b). Here, only small clusters (pairs and triplets) are presented, as the contributions of larger clusters to the ΔH are negligible. For a cluster, positive/negative J_α indicates that the interaction between the same species at the metal sites is repulsive/attractive, and such an atomic arrangement will lead to a positive/negative energy contribution to the formation enthalpy. By analyzing ECIs, as shown in Fig. 2(b), we observed negative J_α values with highest magnitudes for the nearest pair and triplet, indicative of a tendency of clustering but not alloying for neighboring atoms. However, it can be seen that J_α for the next nearest pair is positive, and the magnitude is also comparably high. This makes the mixing of next nearest atoms possible. Therefore, if there exist stable $Ga_{(1-x)}Al_xN$ alloys, clustering in alloys is likely to be observed but only with a cluster size of 2 or 3 atoms.

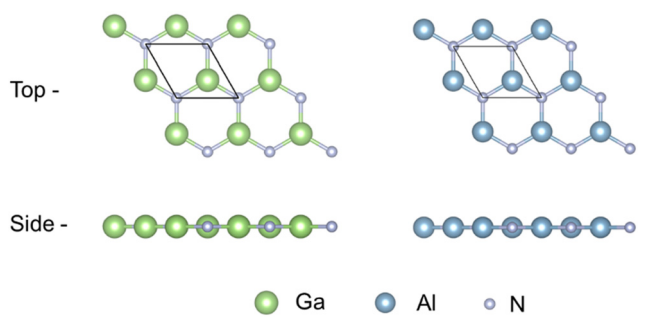

Fig. 1 The top and side views of monolayer III nitrides, where Ga, Al and N atoms are shown in green, blue and grey, respectively.

To further investigate the stability of $Ga_{(1-x)}Al_xN$ alloys, we calculated the phonon dispersion curves of 2×2 $Ga_{0.5}Al_{0.5}N$, which is the alloy configuration predicted to have the highest ΔH among all concentrations (see Fig. S2 in the ESI†). The phonon frequencies are found to be positive, indicating the stability of this alloy structure. Since 2×2 $Ga_{0.5}Al_{0.5}N$ has the highest ΔH and is found to be stable, we can safely assume that all other alloy configurations should be stable. Moreover, since the magnitude of the positive ΔH is very small (below 7 meV), it is anticipated that negative free energies of mixing for alloys can be easily achieved by considering the entropic contributions. We calculated the free energy of mixing for $Ga_{(1-x)}Al_xN$ random alloys. As depicted in Fig. 3, by increasing the temperature to room temperature (300 K), the free energies of random alloys continuously decrease from positive to negative. The critical temperature for complete miscibility is calculated as 85 K, at which temperature the free energies of random alloys in the whole concentration range start to become negative. Therefore, thermodynamically stable $Ga_{(1-x)}Al_xN$ alloys is experimentally achievable.

Electronic properties

As alloying is expected to change the electronic properties of 2D III-nitrides, we then investigated the evolution of the band gap with the composition x for $Ga_{(1-x)}Al_xN$ random alloys. For the calculations of band gap values, HSE06 functionals were used to obtain accurate results. Additionally, we have compared the results for band gaps calculated using HSE06 and PBE functionals to investigate the effect of functional choice, which shows a negligible impact on the band gap trends (see Fig. S5 in the ESI† for details). The band gaps of pristine GaN and AlN are calculated as 3.44 and 4.04 eV respectively, in good agreement with previous works.[11,12] Following the Vegard's law,[38] the lattice constant for alloys should vary linearly with the concentration x. We observed such linearity for $Ga_{(1-x)}Al_xN$ random alloys, as shown in Fig. S3 (ESI†), with the lattice constant decreasing linearly with increasing Al concentration. On the other hand, the dependence of band gap on concentration is often nonlinear and can be described using a quadratic rule:

$$E_g(Ga_{(1-x)}Al_xN) = (1 - x)E_g(GaN) + xE_g(AlN) - bx(1 - x)$$

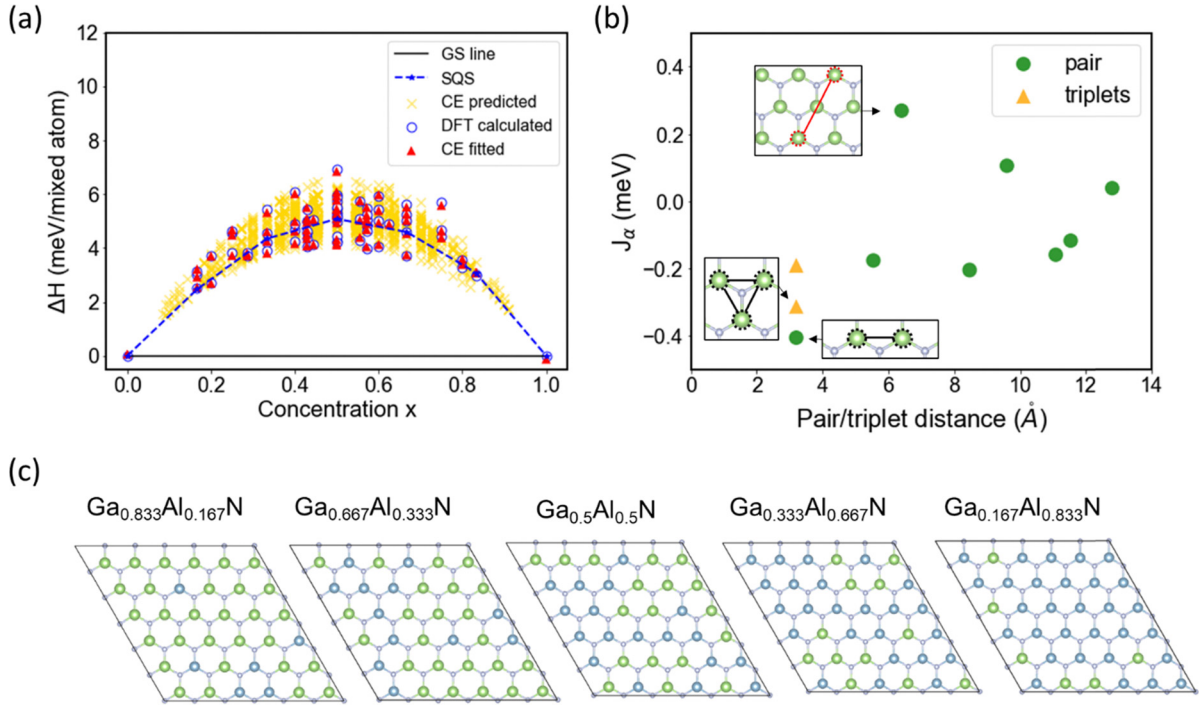

Fig. 2 (a) DFT calculated and cluster expansion fitted results for the formation enthalpies ΔH of $Ga_{(1-x)}Al_xN$ at different concentrations. The ΔH values of ground structures (GS) are shown by a black solid line, and ΔH values of random alloys generated using special quasi-random structure (SQS) method are shown by a blue dashed line. (b) Effective cluster interaction (ECI) J_α for cluster figures, *i.e.*, pairs and triplets, as a function of cluster diameter. (c) Atomic configurations of SQS structures at different concentration, where Ga, Al and N atoms are shown in green, blue and grey.

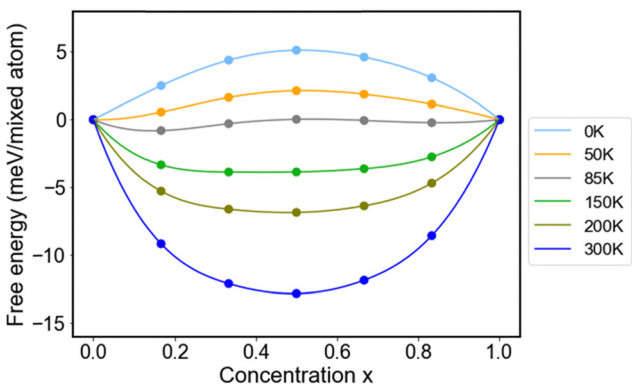

Fig. 3 Free energies of mixing for $Ga_{(1-x)}Al_xN$ random alloys *vs.* concentration x under different temperatures.

where b is the bowing parameter describing the deviation from the linearity. Fig. 4(a) shows that band gaps of random alloys increase nonlinearly with the increasing x. The variation of the band gap comes from the shifting of conduction band minimum (CBM), as shown in Fig. 4(b). By mixing Al into GaN, CBM continuously moves to higher energy levels, while the valence band maximum (VBM) remains nearly constant. The bowing parameter b is calculated as -0.17 eV. We note that in the previous study, the bowing parameter for ordered 2D $Ga_{(1-x)}Al_xN$ alloys was calculated to -0.35 eV.[19] The difference in b values might originate from the different atomic arrangements of alloys. To demonstrate the accuracy of our calculations, 2×2 ordered alloy configurations used in the previous work were utilized to perform band gap calculations, with obtained $b = -0.33$ eV (see Fig. S4, ESI†), comparable to that in the previous work. The results indicate that the ordering effect on the electronic properties of 2D $Ga_{(1-x)}Al_xN$ cannot be neglected. As 2×2 ordered alloy structures consider only the most extreme cases of $Ga_{(1-x)}Al_xN$, random structures used in this work are more likely to be consistent with the real alloys in experiments. Therefore, b values obtained from random alloys are expected to be more accurate to calculate the band gaps of $Ga_{(1-x)}Al_xN$ alloys realized in experiments. Apart from the observed band bowing effect, the continuous changes of band gap values with concentrations also demonstrate that band gap tailoring of 2D III-nitrides is achievable *via* alloying.

To further understand the variations in band gaps, the projected density of states (PDOS) for AlN, GaN, and $Ga_{0.5}Al_{0.5}N$ random alloy were calculated. As shown in Fig. 4(c), it is found that the VBMs in both AlN and GaN are primarily composed of p orbitals from nitrogen atoms. While the contribution of d orbitals from aluminum atoms to the CBM in AlN is still negligible, the d orbitals of gallium atoms in GaN make a significant contribution to the CBM. Therefore, the increased mixing of Ga d orbitals into the CBM of AlN is expected to shift the CBM position downwards, while the VBM position should remain nearly constant, due to the fixed nitrogen concentrations. This is precisely the case for the $Ga_{0.5}Al_{0.5}N$ random alloy. It also explains the evolution of CBM and VBM positions in $Ga_{(1-x)}Al_xN$ with varying concentration x, and that the

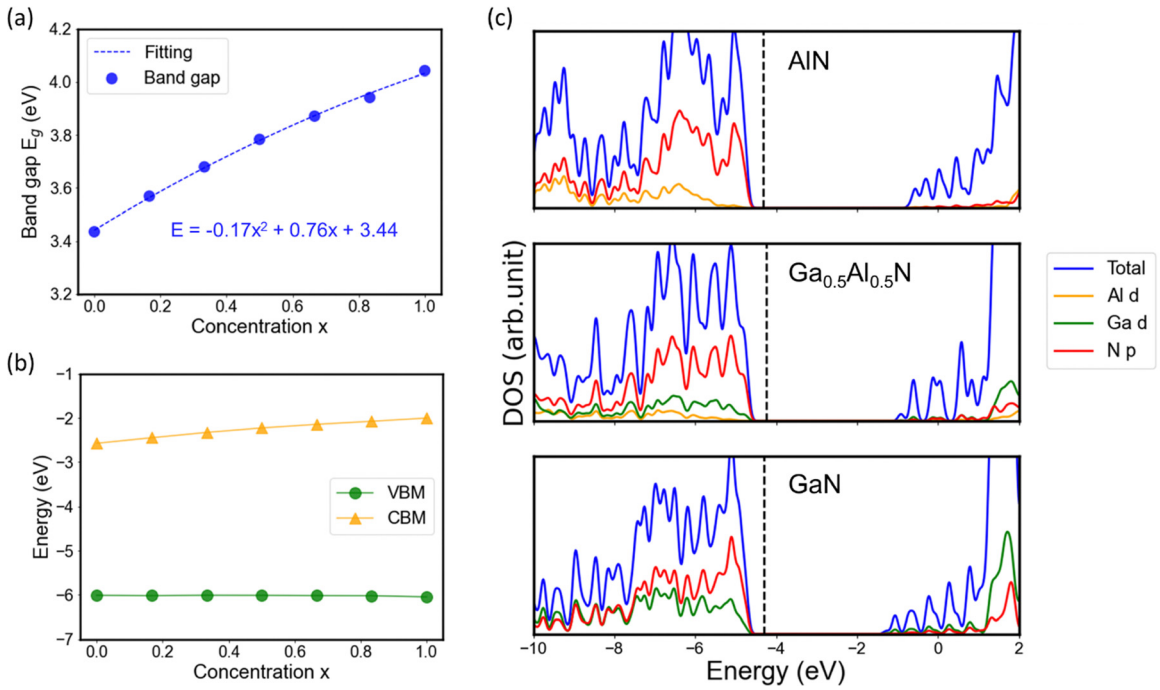

Fig. 4 (a) Band gap E_g of $Ga_{(1-x)}Al_xN$ random alloys as a function of concentration x. (b) The VBM and CBM positions of $Ga_{(1-x)}Al_xN$ random alloys as a function of concentration x. (c) Density of states (DOS) for AlN, GaN and $Ga_{0.5}Al_{0.5}N$ random alloy. Black dashed lines indicate the positions of the Fermi level. Band gaps, VBMs, CBMs and DOS were obtained using HSE06 functionals.

variations of the band gaps mainly arise from the shifting of the CBMs.

Effect of strain

The electronic properties of 2D $Ga_{(1-x)}Al_xN$ under the tensile strain are further investigated, which is of importance for the tuning of physical and chemical properties. We used $Ga_{0.5}Al_{0.5}N$ random alloys as a representative of $Ga_{(1-x)}Al_xN$ alloys and studied the band gap variation under an applied biaxial in-plane tensile strain up to 8% for GaN, AlN and $Ga_{0.5}Al_{0.5}N$. It is noted that such high strains were proven to be affordable for 2D III-nitrides, as previous work observed an 8% strain in stable AlN nanosheets epitaxially grown on Ag(111) substrate.[39] In addition, elastic constants of $Ga_{(1-x)}Al_xN$ random alloys were calculated to further demonstrate their mechanical stabilities (see Table S1 in the ESI† for details). Fig. 5(a) shows the variation of the band gap with applied biaxial strain. It can be seen that the change in the band gap is more significant for GaN than AlN under the same strain. The band gaps decrease monotonically with increasing strains from 3.44 to 1.85 eV for GaN and from 4.04 to 3.12 eV for AlN. By contrast, the effect of strain on the band gaps of $Ga_{0.5}Al_{0.5}N$ is moderate, with band gap values dropping from 3.78 to 2.51 eV up to 8% strain. The VBM and

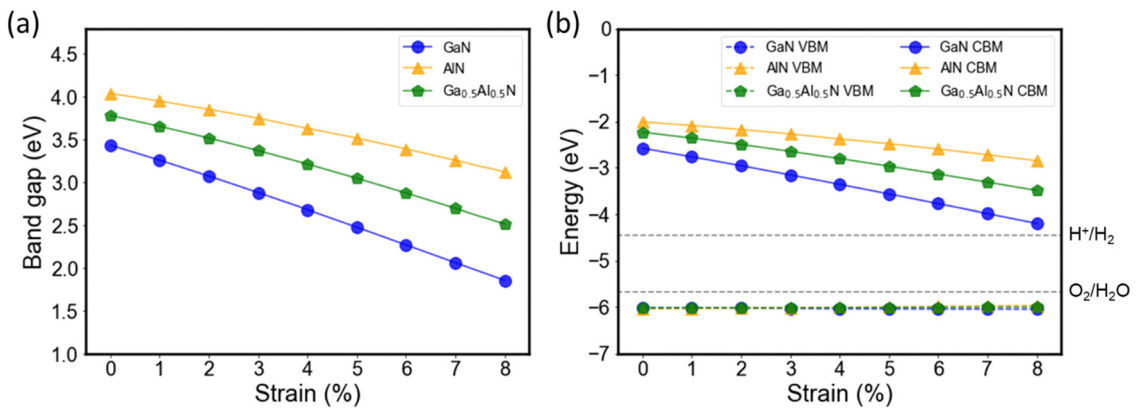

Fig. 5 (a) Band gap values of GaN, AlN and $Ga_{(1-x)}Al_xN$ random alloy as a function of strain. (b) The VBM and CBM positions of GaN, AlN and $Ga_{(1-x)}Al_xN$ random alloy as a function of strain. Black dashed lines indicate the position of potentials of oxidation (O_2/H_2O) and reduction (H^+/H_2) at pH 0 for water splitting. Band gaps, VBMs and CBMs were obtained using HSE06 functionals.

CBM positions of GaN, AlN and $Ga_{0.5}Al_{0.5}N$ under various strains are presented in Fig. 5(b). We can see that after applying strain, for all three structures, CBM positions gradually shift to lower energy levels, contributing to the decreasing band gap values, while the changes in VBM positions are negligible. These results indicate the possibilities of adjusting the electronic properties of 2D $Ga_{(1-x)}Al_xN$ alloys by strain engineering, showing promise for potential novel optoelectronic applications.

Potential applications in photocatalysis

As wide band gap semiconductors, 2D III-nitrides are also potential photocatalysts with appropriate band edge positions for water splitting. To drive two half-reactions of water splitting, *i.e.*, hydrogen evolution reaction (HER) and oxygen evolution reaction (OER), at pH 0, a suitable photocatalyst should have the energy of CBM more positive than −4.44 eV for reduction of H^+ and the energy of VBM more negative than −5.67 eV for oxidation of H_2O.[16] As indicated in Fig. 5(b), GaN, AlN and $Ga_{0.5}Al_{0.5}N$ have suitable band edge positions for water splitting under acidic conditions. Although the applied strains will narrow the band gaps and lower the CBM positions, the CBM positions of III-nitrides are still positive enough for water reduction even at 8% strain. The optical properties of 2D $Ga_{(1-x)}Al_xN$ random alloys were also investigated. The absorption spectra for 2D III-nitrides along x and y directions are shown in Fig. S6 (ESI†). It is found that while the absorption along the x direction shows slightly better absorption compared to the y direction, the absorption for both directions exhibits similar trends with concentration. Specifically, the absorption is enhanced as the Al concentration decreases. This observation is also consistent with the trends observed for band gaps.

Finally, the chemical reactivity on 2D $Ga_{(1-x)}Al_xN$ was explored, using 2D $Ga_{0.5}Al_{0.5}N$ random alloy as a representative (see results for other $Ga_{(1-x)}Al_xN$ random alloys in Fig. S7, ESI†). The free energy pathways of the HER and the OER are shown in Fig. 6(a) and (b), respectively. For the HER, it is found that the hydrogen adsorption configurations on all substrates are similar, with hydrogen atoms adsorbed on top of the N atoms (see Fig. S8 in the ESI†). The calculated ΔG_H for hydrogen adsorption on GaN and AlN are 0.93 and 1.57 eV. As alloying continuously tunes the electronic structures, it is expected that the ΔG_H for $Ga_{0.5}Al_{0.5}N$ should have a value between those for pristine GaN and AlN. The ΔG_H for $Ga_{0.5}Al_{0.5}N$ is calculated as 1.14 eV as expected, closer to that for GaN because the H atom prefers to adsorb on the N atom surrounded by Ga atoms (see Fig. 6(a)). Similar trends can be observed in the case of OER. For all three structures, while oxygen atoms prefer to adsorb on N atoms, *OH and *OOH show stronger adsorption on metal atoms (Fig. S9, ESI†). As shown in Fig. 6(b), the energy difference of the potential limiting step for the OER on $Ga_{0.5}Al_{0.5}N$ has a value between those of pristine GaN and AlN, indicating that the OER activity of $Ga_{0.5}Al_{0.5}N$ falls between that of GaN and AlN. The overpotential for OER on $Ga_{0.5}Al_{0.5}N$ is calculated as 0.87 V. We further investigated the coverage

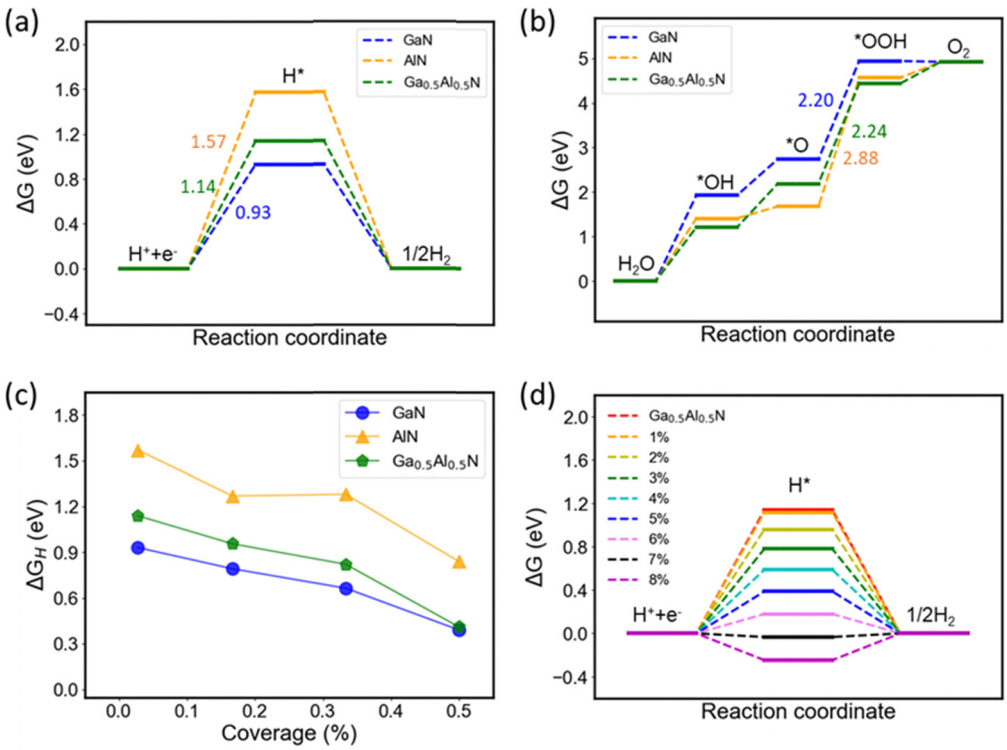

Fig. 6 Calculated Gibbs free energy diagrams for (a) the HER and (b) the OER on the AlN, GaN, and $Ga_{0.5}Al_{0.5}N$ random alloy. (c) ΔG_H on AlN, GaN, and $Ga_{0.5}Al_{0.5}N$ random alloy as a function of hydrogen coverage. (d) Calculated Gibbs free energy diagrams for HER on the $Ga_{0.5}Al_{0.5}N$ random alloy under tensile strains. Free energies were obtained using PBE functionals with DFT-D3 method.

effect on catalytic properties, using HER as an example. As shown in Fig. 6(c), It is found that ΔG_H decreases with increasing hydrogen coverage, showing an enhanced activity with the increasing intermediate coverage.

Additionally, the modifications to the chemical reactivity of 2D III-nitride alloys can further be realized by strain. As depicted in Fig. 6(d), by applying biaxial in-plane tensile strain up to 8%, the ΔG_H for adsorption on 2D $Ga_{0.5}Al_{0.5}N$ random alloy decreases from 1.14 eV to −0.25 eV, indicating a transition of adsorption strength from weak to strong. We note that the ΔG_H for the alloy is close to the thermoneutral value near zero at 7% strain, which demonstrates that optimal catalyst performance on 2D $Ga_{(1-x)}Al_xN$ can be achieved by strain engineering.

Conclusions

In conclusion, density functional theory in conjunction with the cluster expansion method were performed on monolayer $Ga_{(1-x)}Al_xN$ alloys to investigate their stability, and electronic and catalytic properties. Our results show that 2D $Ga_{(1-x)}Al_xN$ alloys are thermodynamically stable. Although positive formation enthalpies ΔH are observed for all alloy configurations, the calculated free energies of alloy formation indicate the complete miscibility in the alloys achieved at only 85 K, far below the room temperature. By analyzing the fitted ECI parameters, the atomic arrangement of alloys was then revealed, showing that Ga/Al atoms tend to mix with the Al/Ga atoms in their next nearest site. On the front of electronic properties, by varying chemical compositions, the band gaps of $Ga_{(1-x)}Al_xN$ random alloys exhibit an apparent bowing effect with bowing parameter b = −0.17 eV, which comes from the variation of CBM positions with alloy concentrations. Besides, we found that biaxial tensile strain can further decrease the band gap values of random alloys significantly, due to its modifications to the CBM positions of alloys. Meanwhile, as potential photocatalysts, $Ga_{(1-x)}Al_xN$ random alloys are confirmed to have suitable band edge positions for water splitting over the entire range of concentration, even under high strains. Finally, on the front of chemical properties, tunable HER and OER properties with varying concentrations are found. Furthermore, by examining hydrogen adsorption on 2D $Ga_{0.5}Al_{0.5}N$ under biaxial strains, we found that $Ga_{0.5}Al_{0.5}N$ is an ideal catalyst for the HER with the Gibbs free energy of hydrogen adsorption ΔG_H close to zero at 7% strain. The present study might guide the future design of electronics and broaden the possible usage of 2D III-nitrides in photocatalysis.

Author contributions

Y. C. and J. S. initiated the project. Y. C. conducted the first-principles calculations. Y. C., P. O. and Z. Y. analyzed the results. Y. C. and J. S. wrote the manuscript with inputs from all the coauthors.

Conflicts of interest

There are no conflicts to declare.

Acknowledgements

This research is supported by the Natural Sciences and Engineering Research Council of Canada (NSERC) Discovery Grant (grant #: NSERC RGPIN-2017-05187) and the McGill Engineering Doctoral Award (MEDA). The authors would also like to acknowledge the Compute Canada and Calcul Québec for providing computing resources.

References

1 S. Mokkapati and C. Jagadish, III-V compound SC for optoelectronic devices, *Mater. Today*, 2009, **12**(4), 22–32.
2 Z. C. Feng, *III-nitride devices and nanoengineering*, World Scientific, 2008.
3 S. Nakamura, T. Mukai and M. Senoh, Candela-class high-brightness InGaN/AlGaN double-heterostructure blue-light-emitting diodes, *Appl. Phys. Lett.*, 1994, **64**(13), 1687–1689.
4 A. V. Akimov, J. T. Muckerman and O. V. Prezhdo, Nonadiabatic Dynamics of Positive Charge during Photocatalytic Water Splitting on GaN(10-10) Surface: Charge Localization Governs Splitting Efficiency, *J. Am. Chem. Soc.*, 2013, **135**(23), 8682–8691.
5 R. T. Rashid, Y. Chen, X. Liu, F. A. Chowdhury, M. Liu, J. Song, Z. Mi and B. Zhou, Tunable green syngas generation from CO2 and H2O with sunlight as the only energy input, *Proc. Natl. Acad. Sci. U. S. A.*, 2022, **119**(26), e2121174119.
6 M. G. Kibria and Z. Mi, Artificial photosynthesis using metal/nonmetal-nitride semiconductors: current status, prospects, and challenges, *J. Mater. Chem. A*, 2016, **4**(8), 2801–2820.
7 D. Wang, A. Pierre, M. G. Kibria, K. Cui, X. Han, K. H. Bevan, H. Guo, S. Paradis, A.-R. Hakima and Z. Mi, Wafer-Level Photocatalytic Water Splitting on GaN Nanowire Arrays Grown by Molecular Beam Epitaxy, *Nano Lett.*, 2011, **11**(6), 2353–2357.
8 H. L. Zhuang, A. K. Singh and R. G. Hennig, Computational discovery of single-layer III-V materials, *Phys. Rev. B: Condens. Matter Mater. Phys.*, 2013, **87**(16), 165415.
9 Z. Y. Al Balushi, K. Wang, R. K. Ghosh, R. A. Vilá, S. M. Eichfeld, J. D. Caldwell, X. Qin, Y.-C. Lin, P. A. DeSario, G. Stone, S. Subramanian, D. F. Paul, R. M. Wallace, S. Datta, J. M. Redwing and J. A. Robinson, Two-dimensional gallium nitride realized via graphene encapsulation, *Nat. Mater.*, 2016, **15**(11), 1166–1171.
10 Z. Huang, T.-Y. Lü, H.-Q. Wang, S.-W. Yang and J.-C. Zheng, Electronic and thermoelectric properties of the group-III nitrides (BN, AlN and GaN) atomic sheets under biaxial strains, *Comput. Mater. Sci.*, 2017, **130**, 232–241.
11 D. Kecik, A. Onen, M. Konuk, E. Gürbüz, F. Ersan, S. Cahangirov, E. Aktürk, E. Durgun and S. Ciraci, Fundamentals, progress, and future directions of nitride-based

semiconductors and their composites in two-dimensional limit: A first-principles perspective to recent synthesis, *Appl. Phys. Rev.*, 2018, **5**(1), 011105.
12 A. Onen, D. Kecik, E. Durgun and S. Ciraci, GaN: From three- to two-dimensional single-layer crystal and its multilayer van der Waals solids, *Phys. Rev. B*, 2016, **93**(8), 085431.
13 C. Bacaksiz, H. Sahin, H. D. Ozaydin, S. Horzum, R. T. Senger and F. M. Peeters, Hexagonal AlN: Dimensional-crossover-driven band-gap transition, *Phys. Rev. B: Condens. Matter Mater. Phys.*, 2015, **91**(8), 085430.
14 E. Gürbüz, S. Cahangirov, E. Durgun and S. Ciraci, Single layers and multilayers of GaN and AlN in square-octagon structure: Stability, electronic properties, and functionalization, *Phys. Rev. B*, 2017, **96**(20), 205427.
15 Q. Chen, H. Hu, X. Chen and J. Wang, Tailoring band gap in GaN sheet by chemical modification and electric field: Ab initio calculations, *Appl. Phys. Lett.*, 2011, **98**(5), 053102.
16 K. Ren, J. Yu and W. Tang, A two-dimensional vertical van der Waals heterostructure based on g-GaN and Mg (OH) 2 used as a promising photocatalyst for water splitting: A first-principles calculation, *J. Appl. Phys.*, 2019, **126**(6), 065701.
17 J.-H. Yang and B. I. Yakobson, Unusual Negative Formation Enthalpies and Atomic Ordering in Isovalent Alloys of Transition Metal Dichalcogenide Monolayers, *Chem. Mater.*, 2018, **30**(5), 1547–1555.
18 S. Susarla, A. Kutana, J. A. Hachtel, V. Kochat, A. Apte, R. Vajtai, J. C. Idrobo, B. I. Yakobson, C. S. Tiwary and P. M. Ajayan, Quaternary 2D Transition Metal Dichalcogenides (TMDs) with Tunable Bandgap, *Adv. Mater.*, 2017, **29**(35), 1702457.
19 M. Kanli, A. Onen, A. Mogulkoc and E. Durgun, Characterization of two-dimensional Ga1−xAlxN ordered alloys with varying chemical composition, *Comput. Mater. Sci.*, 2019, **167**, 13–18.
20 J. M. Sanchez, F. Ducastelle and D. Gratias, Generalized cluster description of multicomponent systems, *Phys. A*, 1984, **128**(1), 334–350.
21 L. G. Ferreira, S.-H. Wei and A. Zunger, First-principles calculation of alloy phase diagrams: The renormalized-interaction approach, *Phys. Rev. B: Condens. Matter Mater. Phys.*, 1989, **40**(5), 3197–3231.
22 A. Van De Walle, M. Asta and G. Ceder, The alloy theoretic automated toolkit: A user guide, *Calphad*, 2002, **26**(4), 539–553.
23 J. Kang, S. Tongay, J. Li and J. Wu, Monolayer semiconducting transition metal dichalcogenide alloys: Stability and band bowing, *J. Appl. Phys.*, 2013, **113**(14), 143703.
24 A. Zunger, S. H. Wei, L. G. Ferreira and J. E. Bernard, Special quasirandom structures, *Phys. Rev. Lett.*, 1990, **65**(3), 353–356.
25 W. R. L. Lambrecht and B. Segall, Anomalous band-gap behavior and phase stability of c-BN--diamond alloys, *Phys. Rev. B: Condens. Matter Mater. Phys.*, 1993, **47**(15), 9289–9296.
26 J. K. Nørskov, J. Rossmeisl, A. Logadottir, L. Lindqvist, J. R. Kitchin, T. Bligaard and H. Jónsson, Origin of the Overpotential for Oxygen Reduction at a Fuel-Cell Cathode, *J. Phys. Chem. B*, 2004, **108**(46), 17886–17892.
27 W. Kohn and L. J. Sham, Self-Consistent Equations Including Exchange and Correlation Effects, *Phys. Rev.*, 1965, **140**(4A), A1133–A1138.
28 G. Kresse and D. Joubert, From ultrasoft pseudopotentials to the projector augmented-wave method, *Phys. Rev. B: Condens. Matter Mater. Phys.*, 1999, **59**(3), 1758–1775.
29 G. Kresse and J. Furthmüller, Efficient iterative schemes for ab initio total-energy calculations using a plane-wave basis set, *Phys. Rev. B: Condens. Matter Mater. Phys.*, 1996, **54**(16), 11169–11186.
30 P. E. Blöchl, Projector augmented-wave method, *Phys. Rev. B: Condens. Matter Mater. Phys.*, 1994, **50**(24), 17953–17979.
31 J. P. Perdew, K. Burke and M. Ernzerhof, Generalized Gradient Approximation Made Simple, *Phys. Rev. Lett.*, 1996, **77**(18), 3865–3868.
32 J. P. Perdew, J. A. Chevary, S. H. Vosko, K. A. Jackson, M. R. Pederson, D. J. Singh and C. Fiolhais, Atoms, molecules, solids, and surfaces: Applications of the generalized gradient approximation for exchange and correlation, *Phys. Rev. B: Condens. Matter Mater. Phys.*, 1992, **46**(11), 6671–6687.
33 A. V. Krukau, O. A. Vydrov, A. F. Izmaylov and G. E. Scuseria, Influence of the exchange screening parameter on the performance of screened hybrid functionals, *J. Chem. Phys.*, 2006, **125**(22), 224106.
34 S. Grimme, J. Antony, S. Ehrlich and H. Krieg, A consistent and accurate ab initio parametrization of density functional dispersion correction (DFT-D) for the 94 elements H-Pu, *J. Chem. Phys.*, 2010, **132**(15), 154104.
35 S. Grimme, S. Ehrlich and L. Goerigk, Effect of the damping function in dispersion corrected density functional theory, *J. Comput. Chem.*, 2011, **32**(7), 1456–1465.
36 D. Wines, F. Ersan and C. Ataca, Engineering the Electronic, Thermoelectric, and Excitonic Properties of Two-Dimensional Group-III Nitrides through Alloying for Optoelectronic Devices ($B_{1-x}Al_xN$, $Al_{1-x}Ga_xN$, and $Ga_{1-x}In_xN$), *ACS Appl. Mater. Interfaces*, 2020, **12**(41), 46416–46428.
37 G. Ceder, A derivation of the Ising model for the computation of phase diagrams, *Comput. Mater. Sci.*, 1993, **1**(2), 144–150.
38 A. R. Denton and N. W. Ashcroft, Vegard's law, *Phys. Rev. A: At., Mol., Opt. Phys.*, 1991, **43**(6), 3161–3164.
39 P. Tsipas, S. Kassavetis, D. Tsoutsou, E. Xenogiannopoulou, E. Golias, S. Giamini, C. Grazianetti, D. Chiappe, A. Molle and M. Fanciulli, Evidence for graphite-like hexagonal AlN nanosheets epitaxially grown on single crystal Ag (111), *Appl. Phys. Lett.*, 2013, **103**(25), 251605.

